Laser printing hierarchical structures with the aid of controlled capillary-driven self-assembly

Yanlei Hu[a,b], Zhaoxin Lao[a], Benjamin P. Cumming[b], Dong Wu[a], Jiawen Li[a], Haiyi Liang[c], Jiaru Chu[a,1], Wenhao Huang[a], and Min Gu[b,1]

[a]Department of Precision Machinery and Precision Instrumentation, University of Science and Technology of China, Hefei, Anhui 230027, China; [b]Centre for Micro-Photonics and Centre for Ultrahigh-Bandwidth Devices for Optical Systems (CUDOS), Faculty of Science, Engineering and Technology, Swinburne University of Technology, Hawthorn, VIC 3122, Australia; and [c]CAS Key Laboratory of Mechanical Behavior and Design of Materials, and Department of Modern Mechanics, University of Science and Technology of China, Hefei, Anhui 230027, China

Capillary force is often regarded as detrimental because it may cause undesired distortion or even destruction to micro/nanostructures during a fabrication process, and thus many efforts have been made to eliminate its negative effects. From a different perspective, capillary force can be artfully used to construct specific complex architectures. Here, we propose a laser printing capillary-assisted self-assembly strategy for fabricating regular periodic structures. Microscale pillars are first produced by localized femtosecond laser polymerization and are subsequently assembled into periodic hierarchical architectures with the assistance of controlled capillary forces in an evaporating liquid. Spatial arrangements, pillar heights, and evaporation processes are readily tuned to achieve designable ordered assemblies with various geometries. Reversibility of the assembly is also revealed by breaking the balance between the intermolecular force and the elastic standing force. We further demonstrate the functionality of the hierarchical structures as a nontrivial tool for the selective trapping and releasing of microparticles, opening up a potential for the development of in situ transportation systems for microobjects.

laser printing | capillary force | self-assembly | hierarchical structures | microobject trapping

People learn from daily life experience that individual filaments can coalesce, as with wet hairs or paintbrushes pulling out of paint. Analogs of this elastocapillary coalescence exist and are often amplified in micro/nanoelectromechanical system manufacturing processes because the capillary force tends to dominate over the standing force that needs to be overcome for coalescence when the scale is reduced (1, 2). When one aims to create slender structures, the dominant capillary force drives them to collapse, cluster, or be completely destroyed. Some efforts such as adopting a supercritical-point dryer (3, 4) have been made to eliminate these unwanted behaviors when fabricating high-aspect-ratio structures. However, from another point of view, the capillary-driven bottom-up self-assembly can be exploited as a valuable tool to construct complex architectures. Compared with other driving forces for self-assembly such as magnetism (5), electrostatic force (6), and gravity (7), capillary force self-assembly features the advantage of simplicity, low cost, scalability, and tunability.

The desire for scalable and cost-effective self-assembly schemes comes from observations of the natural world, where self-assembled filamentous structures with mechanical compliance at the microscopic and mesoscopic scale are ubiquitous and include, to name a few, actin bundles (8), gecko feet hairs (9), and *Salvinia* leaf (10). These structures give rise to diverse functions ranging from mechanical strengthening (11) and directional adhesion (12, 13) to superhydrophobicity (14) and structural colors (15), thus inspiring researchers to devote their efforts to mimic these multifunctional structures for decades. Many top-down fabrication approaches such as photolithography together with deep dry etching (16), replica molding (14, 17), multibeam laser interference

lithography (18, 19), and electron-beam lithography (20) have been used in combination with capillary force self-assembly to produce hierarchical structures. However, these methods are either high-cost because of the expensive facilities or labor-intensive and time-consuming owing to the multistep patterning and etching procedure.

One approach that overcomes these limitations in producing microfilament structures is the laser printing technique, owing to its speed, simplicity, and inherent flexibility. Particularly, laser printing based on femtosecond laser-induced physicochemical reactions can confine the fabrication to the nanometer domain beyond the light-diffraction limit owing to the two-photon absorption process (21–23), making it a promising tool for fabricating nanobristles. To our knowledge, laser printing has not yet been used together with elastocapillary interaction for producing designable fibrillar assemblies.

Here, we develop a laser printing capillary-assisted self-assembly (LPCS) strategy to realize designable hierarchical functional structures. Intentional asymmetric spatial arrangement and controllable height design are introduced to direct the self-assembly process to generate diverse architectures. A gravity-governed evaporation front approach is also used to form anisotropic assemblies. This strategy exhibits great flexibility and high reliability because the prepared assemblies possess controllable shapes and stable configurations. Moreover, as a proof-of-concept demonstration, the assemblies are used as a versatile tool for the selective trapping and releasing of microparticles, suggesting their further applications in the fields of microobject manipulation, filtration, and transportation.

Laser Printing Micropillar Arrays

Micropillars can be readily fabricated by focusing a femtosecond laser beam into a photosensitive polymer using an objective lens,

APPLIED PHYSICAL SCIENCES

as schematically shown in Fig. 1*A*. The photopolymer is mounted on a 3D nanotranslation stage to determine the pillars location and height. Fig. 1 *B* and *C* show SEM images of a standing micropillar array with equal spacing (5 μm) between them. The diameter of each pillar is 760 nm at the bottom and the height is 2.5 μm. The tip of each pillar is found to have a radius of 100 nm (Fig. 1*C*, *Inset*).

Dynamics of the Capillary Force-Induced Self-Assembly

The height of pillars and distance between them can be conveniently controlled by moving the nanotranslation stage in the vertical and horizontal directions during photopolymerization. As the pillar height is increased, individual pillars are found to be bent and stuck to each other at their top ends, as shown in Fig. 1*E*. The joining is due to the evaporation-induced capillary force present during the subsequent developing process needed to wash away the polymer that was not exposed to the laser (the details of micropillar fabrication and sample development are presented in *Materials and Methods* and *Supporting Information, section S1* and *Fig. S1*. All characterization methods are described in *Supporting Information, section S2*).

As the developer evaporates to the level of the freestanding tips, a meniscus is formed between neighboring pillars, yielding a capillary force (24), $F_C \sim \gamma r^2 \cos^2\theta/d$, which is proportional to the interfacial tension γ of the solvent, the square of the radius r of the pillars, and the squared cosine of contact angle θ and inversely proportional to the spacing d between adjacent pillars, as shown in Fig. 1*D*. Resistance to the capillary force is the bending ability of pillars, giving rise to an elastic restoring force upon contact just at their tips, $F_S \sim Er^4 d/h^3$, where E is Young's modulus and h is the height of the pillars. A quantitative discussion on the capillary force and the standing force is given in *Supporting*
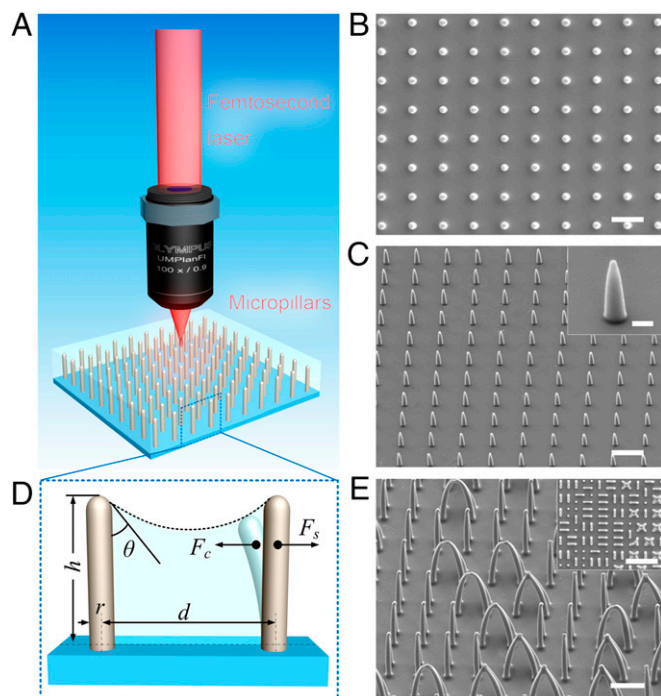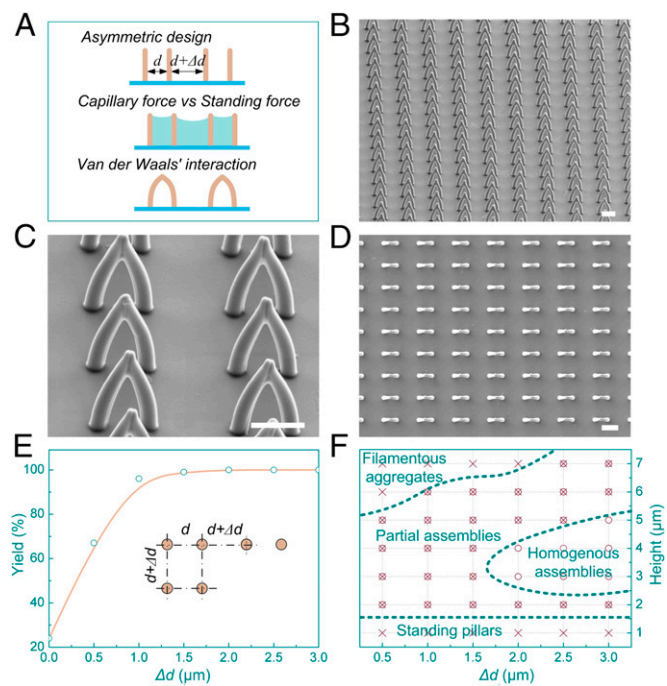

Fig. 2. Controllable LPCS process. (*A*) Schematic diagram showing the method of tuning capillary force by controlling the spacing distribution of pillars. (*B* and *C*) Angled view and magnified view of two-pillar assemblies. (Scale bars, 5 μm and 3 μm, respectively.) (*D*) Top view of the assembled two-pillar cells. (Scale bar, 5 μm.) (*E*) Quantitative study on the yield as a function of Δ*d*. The distance variations exist in both horizontal and vertical directions, as shown in the inset illustration. (*F*) Dependence of different types of assemblies on Δ*d* and *h* (plotted from Table S1).

Information, section S3. A balance between the capillary force and the standing force reaches a critical distance d_c, below which neighboring pillars can be assembled together, or otherwise remain upright. For a given pillar height h, two neighboring pillars can remain contacting when $d < d_c$ by either capillary forces F_c during liquid drying or the short-range van der Waals forces F_v in air. In the case of more than two pillars, the critical assembly condition can be expected to retain the same scaling form (24). For the assembly of an arbitrarily arranged pillar forest, the system can be also explored by a global energy minimization theory, which posits that the final equilibrium state tends to reach a minimum energy state under the action of various forces (25).

From the formula of the elastic standing force we can see that F_s is inversely proportional to the cube of height h. Hence, the short pillar array in Fig. 1 *B* and *C* survives in the drying process whereas most of the longer pillars shown in Fig. 1*E* adhere to one or more of their neighbors. It is important to note that for an isolated pillar in the center of an equally spaced square lattice the capillary forces from each direction are identical and finely balanced. However, random imperfections in pillar structures or instabilities in the evaporating process can break the weak balance and induce uncontrolled bending. Therefore, the assembled pattern of the symmetric square array is random and individual standing pillars and two-, three-, or four-pillar cells are likely to be formed without distinct regularity (Fig. 1*E*, *Inset*).

Controlled LPCS Process

To reduce the formation of these unwanted irregular structures and to provide a level of control over the self-assembly process, it is necessary to finely tune the relationship between the capillary and elastic forces to direct the self-assembly as desired. One possible method is to locally vary the strength of the capillary

Fig. 1. Laser printing of uniformly distributed micropillar arrays. (*A*) Schematic illustration of the laser printing of a micropillar array. (*B* and *C*) Top and tilted SEM views of the as-prepared micropillar arrays, with a height of 2.5 μm. (Scale bars, 5 μm.) Inset of *C* is a magnified view of an individual pillar. (Scale bar, 700 nm.) (*D*) Illustration of the forces interacting on the pillars during the liquid evaporation. (*E*) Capillary force-induced random self-assembly of micropillars by increasing their heights. (Scale bar, 5 μm.) (*Inset*) Top view of the self-assembled structures. (Scale bar, 20 μm.)
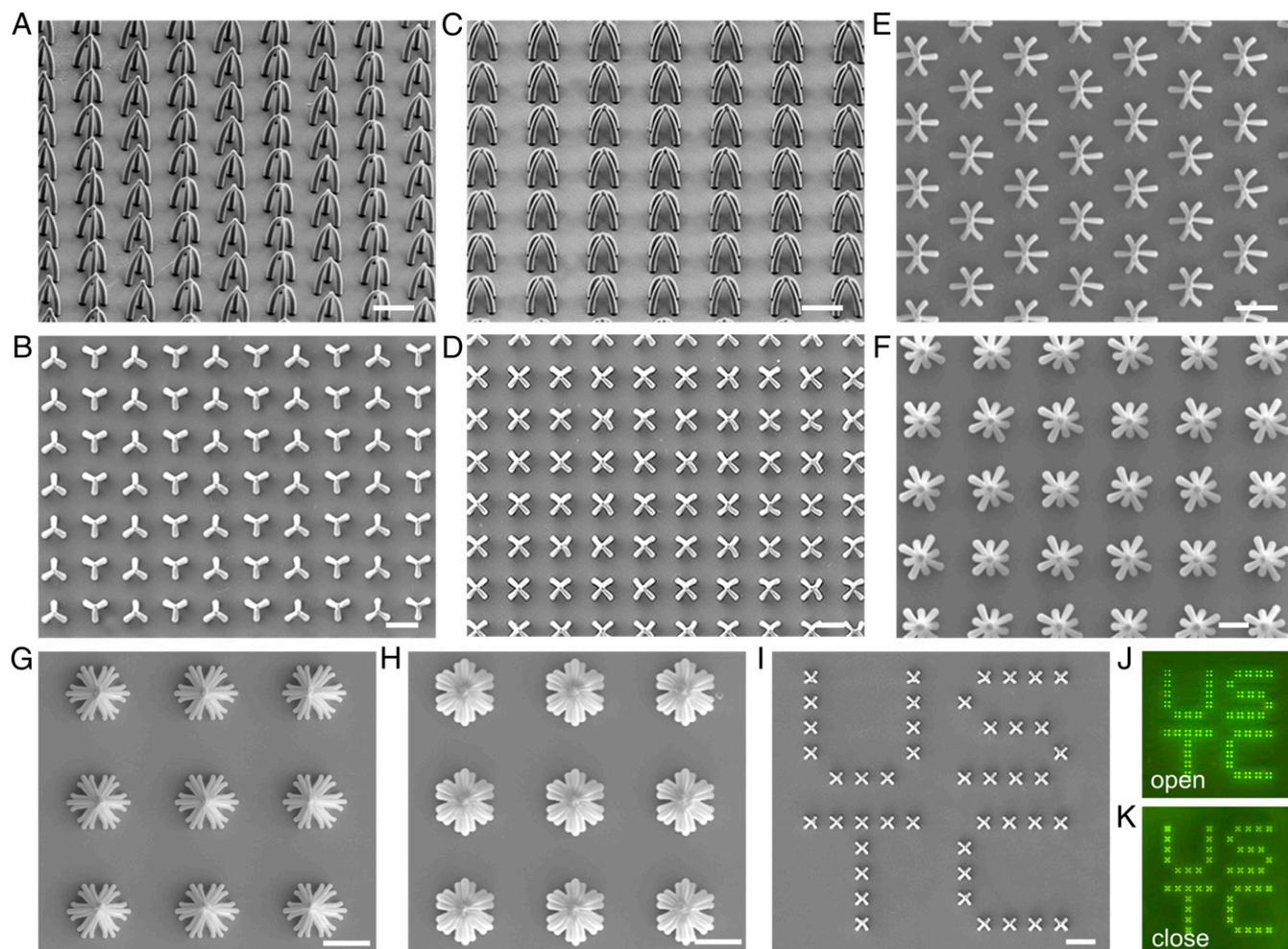
Fig. 3. Examples of the diverse ordered structures prepared by the LPCS approach. (*A* and *B*) Angled and top views of three-pillar cells. (*C* and *D*) Angled and top views of four-pillar cells. (*E*) Six-pillar cells with hexagonal arrangement. (*F*) Nine-pillar cells with three different rotations: 0°, 30° and 60°, respectively. (*G* and *H*) Daisy-like structures consisting of 25 pillars in each cell. Different exposure powers, 75 mW and 85 mW, are used for *G* and *H*, respectively. (*I*) Four-pillar cells are assembled along a specific route and a "USTC" pattern is formed. (Scale bars, 10 μm.) (*J* and *K*) Fluorescence microscopic images of *I* during liquid drying, indicating the open and closed states respectively.

force by introducing an asymmetric arrangement design, such as by maintaining a constant distance *d* between pillars destined for self-assembly, and introducing an additional spacing, Δd, between separate self-assembled sets. Schematically, this is depicted in the one-dimensional case in Fig. 2*A*, where the interpillar spacing is tailored and hence the pillars bend along a defined direction under an unbalanced capillary force. Uniform predesigned periodic two-pillar structures for the case of $h = 4$ μm, $d = 3$ μm, and $\Delta d = 2$ μm are shown in Fig. 2 *B* and *D*. From the magnified SEM image in Fig. 2*C*, we can see that the two tips of pillars adhere steadily to each other after liquid evaporation, implying the short-range van der Waals force is strong enough to accommodate the elasticity and thus retain a stable bent configuration (i.e., $F_v > F_s$).

To systematically study the engineered LPCS process, we further perform a yield test by printing a series of pillar arrays with different intercell spacing variations Δd and heights h. First, considering the pillar arrays with a constant height of 4 μm and intracell pitch of 3 μm (shown in Fig. 2*E*), the pillars bend randomly and only ~24% of them assemble into two-pillar cells when there is no spacing variation ($\Delta d = 0$). As Δd increases, the yield rate of the expected two-pillar cells rises sharply, reaching 98% at $\Delta d = 1$ μm and 100% at $\Delta d = 2$ μm. Repeated

experiments are carried out to verify the reliability. In the case of $\Delta d = 2$ μm, all pillars without exception assemble into the intended two-pillar cells, indicating the method is feasible to produce robust, uniform, and ordered assemblies.

In addition to controlling the capillary force by varying the interpillar distance, according to the elasticity equation, controlling the height of pillars provides another means to tune the elastic force for designable LPCS. When the pillars are too short (1 μm), they can stand vertical to the substrate regardless of the intercell spacing. When the pillars are too high (e.g., >6 μm), filamentous aggregates with various nucleated centers may be generated (Fig. S2). Only in the case of suitable combinations of heights and intercell spaces (for example when *h* are between 3 μm and 4 μm, and Δd is larger than 2 μm) can large-area homogenous ordered assemblies be formed. For most of the parameter space in Fig. 2*F*, only part of pillars make up designed assemblies whereas the others remain straight or form filamentous aggregates. Therefore, four independent regions can be classified to differentiate LPCS configurations, providing us a quantitative reference for developing uniform hierarchical structures. It is worth mentioning that the fabrication time for one pillar is only 0.2 s, and the total time for fabricating a 200-μm × 200-μm area is less than 10 min.
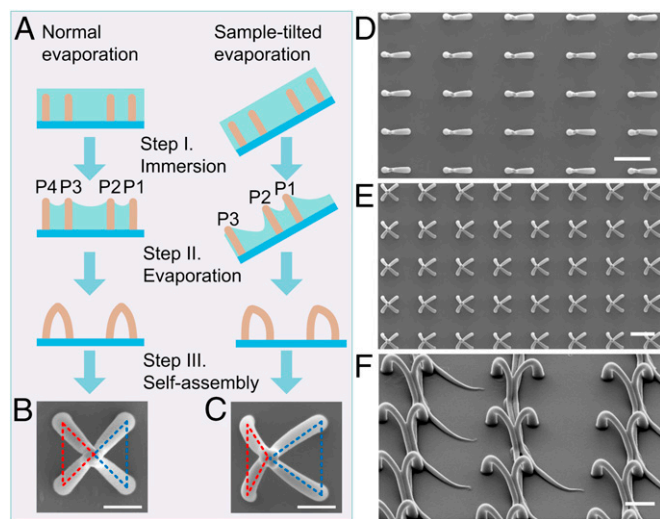
Fig. 4. Evaporation front-directed LPCS method for obtaining anisotropic assemblies. (*A–C*) Schematic diagram for the comparison between normal evaporation and sample-tilted evaporation and corresponding assembled results. (Scale bars, 2 μm.) (*D–F*) SEM images of the anisotropic assemblies with different cells: two-pillar, four-pillar and ultra-long two-pillar (12 μm). (Scale bars: *D* and *E*, 5 μm; *F*, 2 μm.)

Preparation of Diverse Hierarchical Architectures

Owing to the high flexibility of the laser printing technique, more complex hierarchical assemblies can be achieved based on the asymmetric capillary force. Fig. 3 shows a series of assemblies with multielement cells. The tilted views of the SEM images of three- and four-pillar assemblies (Fig. 3 *A* and *C*) show fine replication results of the laser printing and high uniformity of the 3D self-assembled structures. A six-pillar cell array with hexagonal arrangement and nine-pillar cell arrays with different sizes and rotational angles are also designed and shown in Fig. 3 *E* and *F* and Fig. S3. In some LPCS configurations, the boundary pillars in a square array tend to assemble into cells with a higher number of pillars owing to relatively larger capillary force (Fig. S2).

Assemblies with a large number of pillars are also possible via LPCS. Daisy-like structures with 25 pillars arranged in the sixfold symmetry geometry are successfully formed, as shown in Fig. 3 *G* and *H*. Similar to electron beam lithography (20), the exposure dose can also be controlled to obtain structures with tunable diameter and elasticity, contributing to different assembly configurations. The self-assembled pillar cells can be further arranged in arbitrary patterns (Fig. 3*I* and Fig. S3), exhibiting the great flexibility of the LPCS method. Furthermore, because the assemblies are retained by the van der Waals force in air, it is possible to break the balance between the short-range intermolecular force and the elastic standing force to return the assemblies to their initial state. A simple method of reversal involves the immersion of the structures in a liquid such that the van der Waals force between pillars decreases sharply and instead a new van der Waals force between pillars and liquid arises. Note that the pillar–liquid intermolecular van der Waals force exists in all directions around the pillar and ultimately they cancel each other out. Under these circumstances the pillars recover under their own elastic standing force. The reversible opening and closing of the assemblies is shown in Fig. 3 *J* and *K*, taken by a fluorescence microscope, and can also be observed via an optical microscope (Movie S1).

Anisotropic LPCS Structures

Hierarchical structures with controlled anisotropy or chirality are highly desired in biological and photonic applications (26, 27). Chiral assemblies have been prepared and studied by

Aizenberg and coworkers (16) and also observed in our experiments when the micropillars are of sufficient height (Fig. S4). Here we focused on the anisotropy control of the assemblies. To obtain anisotropic assembled cells, an evaporation front-directed method can be applied during the sample development. The operation is as simple as tilting the substrate when the development is just about to be finished, as depicted in Fig. 4*A*. One end of the sample is immersed in the developing solvent and the other end is exposed to the air so that the evaporation front is directed to move from one side to the other, parallel to the substrate surface. Owing to the gravity-governed capillary force difference, anisotropic assemblies are obtained over the entire pillar array, as shown in Fig. 4 *D–F*.

Selective Trapping and Releasing of Microobjects

So far, we have shown that our LPCS method is capable of producing highly repeatable and large-scale hierarchical structures. One possible application of these structures is in microobject trap-release systems, which are intensively demanded in the fields of chemical analysis and biomedical devices and have drawn considerable attention from researchers. Some studies have revealed that the fibrillar structures exhibit wondrous adhesive or trapping properties in biological systems such as those of the beetle (28) and gecko (29, 30). These kinds of bioinspired adhesive filaments can be developed in various technical applications. As an example, the capillary force-assembled flexible nanofingers can be creatively used to form hot spots for molecule detection and identification based on surface-enhanced Raman spectroscopy (31, 32). Although optical tweezers are able to manipulate small objects with different sizes ranging from tens of nanometers to micrometers, a substantial mechanical gripper is still desired in the absence of an energy beam and free of possible harm to living samples or influences to chemical reactions. Examples include miniaturized self-folding grippers that are actuated by differential residual stress (33), magnetic force (34), temperature (35, 36), and chemicals (37, 38). We show here our LPCS artificial fibrillar structures are capable of capturing microparticles with excellent selectivity. The particles can be trapped inside the "cage-like" spaces constructed from four bent pillars by capillary force. Furthermore, the size of the particles to be captured can be controlled by adjusting the intracell pitch of the assemblies.

The concept of selective trapping is sketched in Fig. 5*A*. Only those particles of suitable size can be effectively caught owing to the space limitation of the microgripper. Particles too large in size are unable to enter the intracell space and can be blocked from trapping. Small particles can move freely in and out the structures without being trapped. An experimental demonstration is shown in Fig. 5*B*, from which we can see that the particle with diameter of 2 μm is trapped by the four-claw mechanical gripper, and the other particles with diameters too large (3.2 μm) or too small (1 μm) are not trapped. For practical filtration applications, the unwanted particles outside the LPCS structures can be cleaned out by external force (e.g., blown away by compressed air). Owing to the design flexibility of our LPCS technique, the intracell pitch between adjacent pillars can be easily changed to trap specific particles. For example, assembled cells with pitch of 3.9 μm can be used to efficiently trap 3.8-μm microparticles, as shown in Fig. 5*C*. To further investigate the trapping ability of the artificial microgripper, we prepared a series of assemblies to trap various particles, from 1 μm to 4.6 μm. As shown in Fig. 5*D*, microparticles with different sizes can be trapped by tuning the intracell pitches accordingly. To ensure efficient trapping, the required intracell distance must approximately equal to the particle size.

Apart from the size selectivity, the trapping efficiency is an important factor to evaluate the trapping performance. Here we define the trapping efficiency as the ratio of the assembled cells that trap particles with success to the total number of cells.
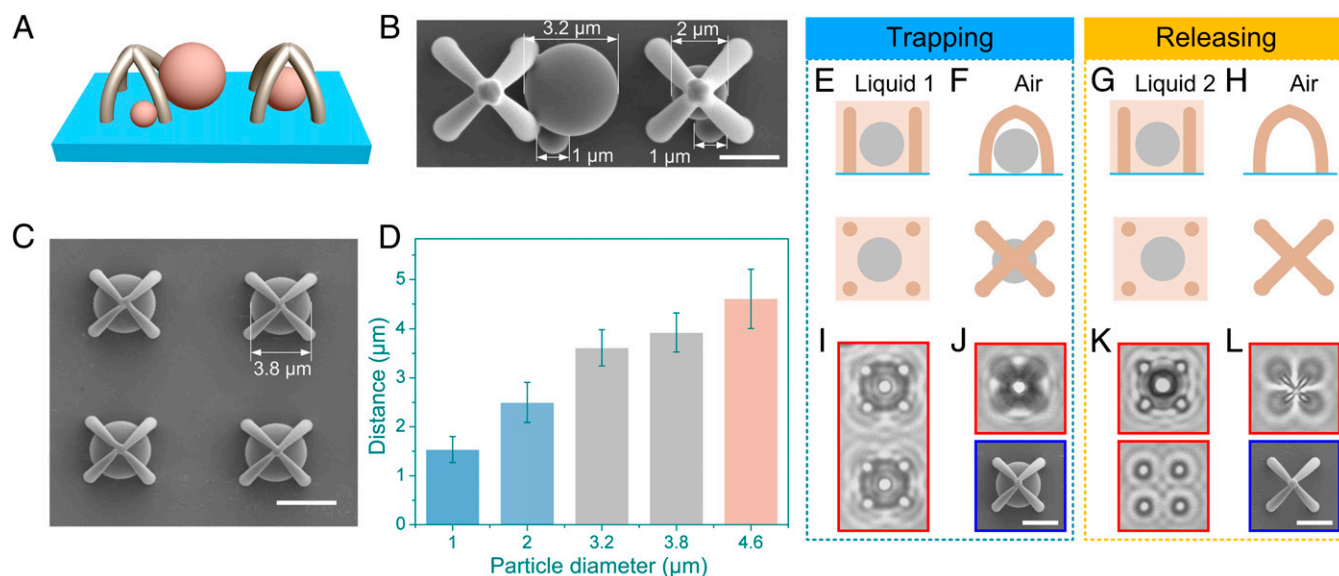
Fig. 5. Demonstration of the selective microparticle trapping, releasing, and transportation ability of the LPCS microstructures. (*A*) Illustration of the concept of microobject selective trapping. (*B*) Experimental demonstration of selective trapping of microparticles. (Scale bar, 2 μm.) (C) Trapping of 3.8-μm particles by tuning the size of the LPCS mechanical gripper. (Scale bar, 4 μm.) (*D*) Relationship between the particle diameter and the intracell distance of the microstructures that can trap the corresponding particles effectively. (*E–H*) Schematics of particle transportation using the LPCS structures. (*I–L*) Microscope images of microstructures and microparticles corresponding to different stages of transportation. Red frames indicate optical images and blue ones indicate SEM images. (Scale bars, 3 μm.)

According to our experiments, the trapping efficiency is ~35% and can be further improved by increasing the microparticle concentration. It is interesting that the presence of particles also affects the elastocapillary interaction, which further benefits the trapping efficiency because the new capillary force inside the cell makes the particle much easier to trap (*Supporting Information, section S4* and Fig. S5).

Microobject controllable releasing is another desirable function for chemical and cell biological applications. As mentioned above, the capillary-driven self-assembly is reversible, and when the assemblies are put into liquid again the bent pillars can return to their original standing state, causing the grippers to open. The trapped microparticles can thus escape and be released, as sketched in Fig. 5 *E–H*. It is worth mentioning that the as-prepared grippers can be reused and exhibit no obvious functional degradation after over a dozen repetitions. The selective trapping and releasing process is also applicable for microobjects with arbitrary shapes and surface properties.

As a proof-of-concept demonstration, we fabricate a micropillar array with an intracell pitch of 3.9 μm and then put it into a solvent (1-propanol) consisting of three different particles of sizes 2, 3.8, and 4.6 μm. After withdrawal from the solvent and the drying procedure, only the 3.8-μm particles are captured by the capillary-driven grippers (Fig. 5 *I* and *J*). Then we move the pillar assemblies together with the selected particles into another solvent (e.g., acetone). The grippers open and the selected particles are released into the new solvent (Fig. 5 *K* and *L*). This ability of microobject selective transportation may find wide applications owing to its scalability, designability, and reproducibility.

In summary, we have demonstrated an LPCS method for realizing hierarchical periodic microstructures. Various microarchitectures are designed and constructed by tuning the capillary force and elastic standing force through spatial arrangements and pillar heights, respectively. Complicated assemblies can be achieved owing to the high flexibility of the LPCS method. Anisotropic assemblies can also be obtained by the evaporation front-directed method. This top-down/bottom-up hybrid strategy for preparing hierarchical structures features simplicity, scalability, and high flexibility in comparison with other state-of-the-art

approaches such as photolithography (39), electron-beam lithography (20, 40), and template replicating (4, 16). Moreover, the assembled cells can be used as automatic microgrippers for selective trapping and controllable releasing of microobjects, suggesting numerous potential applications in the fields of chemistry, biomedicine, and microfluidic engineering.

Materials and Methods

Additional details can be found in *Supporting Information, section S1.*

LPCS Fabrication of Micropillar Arrays. A typical femtosecond laser direct writing system is used for producing micropillar arrays, in which a Ti:sapphire laser oscillator (Chameleon vision-S; Coherent) is used as the light source, operating at a central wavelength of 800 nm, with a repetition rate of 80 MHz and a pulse duration of 75 fs. A 100× objective (Olympus) with N.A. 0.9 is used to focus the laser beam inside the photosensitive material. A commercially available zirconium–silicon hybrid sol-gel material is used for photopolymerization (SZ2080; provided by IESL-FORTH). The detailed synthesis process is described elsewhere (41, 42). The principal advantage of this material in comparison with other photoresists is the negligible shrinkage during structuring. After polymerization, the sample is developed in 1-propanol for 20 min until all of the unpolymerized parts are washed away. After withdrawal from 1-propanol, the liquid layer on the sample surface evaporates and induces the micropillar array to assemble into highly ordered structures with the aid of accompanying capillary force.

Microparticle Trapping and Releasing. Polystyrene microspheres with diameters of 1, 2, 3.2, 4.6, and 5.8 μm were synthesized by Wakely Scientific Corp. Inc. and used as received. For microparticle trapping, the sample with LPCS arrays is put into the solvent (1-propanol) containing microspheres and then withdrawn after a while. After solvent evaporation, only the suitable microparticles were trapped by adjacent pillars due to the capillary force. Relatively large assembled cells may cause the trapping of multiple particles and long filamentous assemblies can trap particles without selectivity (Fig. S6). Although high microsphere concentration benefits the trapping efficiency, too high a concentration (>10^{-3} g/mL) may result in particle aggregation, as shown in Fig. S7.

For the controlled releasing of microparticles, the sample is placed inside liquid and a slight vibration is applied to speed up the opening of the microassemblies and release of the microparticles.

1. Storm AJ, Chen JH, Ling XS, Zandbergen HW, Dekker C (2003) Fabrication of solid-state nanopores with single-nanometre precision. *Nat Mater* 2(8):537–540.
2. Chiodi F, Roman B, Bico J (2010) Piercing an interface with a brush: Collaborative stiffening. *Europhys Lett* 90(4):44006.
3. DeSimone JM (2002) Practical approaches to green solvents. *Science* 297(5582):799–803.
4. Zhang Y, Lo C-W, Taylor JA, Yang S (2006) Replica molding of high-aspect-ratio polymeric nanopillar arrays with high fidelity. *Langmuir* 22(20):8595–8601.
5. Grzybowski BA, Stone HA, Whitesides GM (2000) Dynamic self-assembly of magnetized, millimetre-sized objects rotating at a liquid-air interface. *Nature* 405(6790):1033–1036.
6. Willerich I, Gröhn F (2010) Photoswitchable nanoassemblies by electrostatic self-assembly. *Angew Chem Int Ed Engl* 49(44):8104–8108.
7. Stauth SA, Parviz BA (2006) Self-assembled single-crystal silicon circuits on plastic. *Proc Natl Acad Sci USA* 103(38):13922–13927.
8. Cohen AE, Mahadevan L (2003) Kinks, rings, and rackets in filamentous structures. *Proc Natl Acad Sci USA* 100(21):12141–12146.
9. Autumn K, et al. (2000) Adhesive force of a single gecko foot-hair. *Nature* 405(6787):681–685.
10. Barthlott W, et al. (2010) The salvinia paradox: Superhydrophobic surfaces with hydrophilic pins for air retention under water. *Adv Mater* 22(21):2325–2328.
11. Lee JA, et al. (2014) All-solid-state carbon nanotube torsional and tensile artificial muscles. *Nano Lett* 14(5):2664–2669.
12. Kwak MK, Jeong HE, Bae WG, Jung H-S, Suh KY (2011) Anisotropic adhesion properties of triangular-tip-shaped micropillars. *Small* 7(16):2296–2300.
13. Pang C, et al. (2012) Bioinspired reversible interlocker using regularly arrayed high aspect-ratio polymer fibers. *Adv Mater* 24(4):475–479.
14. Chandra D, Taylor J, Yang S (2008) Replica molding of high-aspect-ratio (sub-) micron hydrogel pillar arrays and their stability in air and solvents. *Soft Matter* 4(5):979–984.
15. Nawrot M, Zinkiewicz L, Włodarczyk B, Wasylczyk P (2013) Transmission phase gratings fabricated with direct laser writing as color filters in the visible. *Opt Express* 21(26):31919–31924.
16. Pokroy B, Kang SH, Mahadevan L, Aizenberg J (2009) Self-organization of a mesoscale bristle into ordered, hierarchical helical assemblies. *Science* 323(5911):237–240.
17. Chandra D, Yang S (2010) Stability of high-aspect-ratio micropillar arrays against adhesive and capillary forces. *Acc Chem Res* 43(8):1080–1091.
18. Wu D, et al. (2013) Rapid, controllable fabrication of regular complex microarchitectures by capillary assembly of micropillars and their application in selectively trapping/releasing microparticles. *Small* 9(5):760–767.
19. Wu D, et al. (2009) Self-organization of polymer nanoneedles into large-area ordered flowerlike arrays. *Appl Phys Lett* 95(9):091902.
20. Duan H, Berggren KK (2010) Directed self-assembly at the 10 nm scale by using capillary force-induced nanocohesion. *Nano Lett* 10(9):3710–3716.
21. Kawata S, Sun H-B, Tanaka T, Takada K (2001) Finer features for functional microdevices. *Nature* 412(6848):697–698.
22. Gan Z, Cao Y, Evans RA, Gu M (2013) Three-dimensional deep sub-diffraction optical beam lithography with 9 nm feature size. *Nat Commun* 4:2061.
23. Hu Y, et al. (2012) Femtosecond laser induced surface deformation in multidimensional data storage. *Appl Phys Lett* 101(25):251116.
24. Chandra D, Yang S (2009) Capillary-force-induced clustering of micropillar arrays: Is it caused by isolated capillary bridges or by the lateral capillary meniscus interaction force? *Langmuir* 25(18):10430–10434.
25. Wei Z, et al. (2015) Elastocapillary coalescence of plates and pillars. *Proc R Soc Lond A*, 10.1098/rspa.2014.0593.
26. Aggeli A, et al. (2001) Hierarchical self-assembly of chiral rod-like molecules as a model for peptide β -sheet tapes, ribbons, fibrils, and fibers. *Proc Natl Acad Sci USA* 98(21):11857–11862.
27. Turner MD, et al. (2013) Miniature chiral beamsplitter based on gyroid photonic crystals. *Nat Photonics* 7(10):801–805.
28. Eisner T, Aneshansley DJ (2000) Defense by foot adhesion in a beetle (Hemisphaerota cyanea). *Proc Natl Acad Sci USA* 97(12):6568–6573.
29. Geim AK, et al. (2003) Microfabricated adhesive mimicking gecko foot-hair. *Nat Mater* 2(7):461–463.
30. Peattie AM, Full RJ (2007) Phylogenetic analysis of the scaling of wet and dry biological fibrillar adhesives. *Proc Natl Acad Sci USA* 104(47):18595–18600.
31. Hu M, et al. (2010) Gold nanofingers for molecule trapping and detection. *J Am Chem Soc* 132(37):12820–12822.
32. Ou FS, et al. (2011) Hot-spot engineering in polygonal nanofinger assemblies for surface enhanced Raman spectroscopy. *Nano Lett* 11(6):2538–2542.
33. Malachowski K, et al. (2014) Self-folding single cell grippers. *Nano Lett* 14(7):4164–4170.
34. Sakar MS, et al. (2010) Single cell manipulation using ferromagnetic composite microtransporters. *Appl Phys Lett* 96(4):043705.
35. Leong TG, Randall CL, Benson BR, Zarafshar AM, Gracias DH (2008) Self-loading lithographically structured microcontainers: 3D patterned, mobile microwells. *Lab Chip* 8(10):1621–1624.
36. Azam A, Laflin KE, Jamal M, Fernandes R, Gracias DH (2011) Self-folding micropatterned polymeric containers. *Biomed Microdevices* 13(1):51–58.
37. Leong TG, et al. (2009) Tetherless thermobiochemically actuated microgrippers. *Proc Natl Acad Sci USA* 106(3):703–708.
38. Bassik N, et al. (2010) Enzymatically triggered actuation of miniaturized tools. *J Am Chem Soc* 132(46):16314–16317.
39. Segawa H, Yamazaki Y, Yano T, Shibata S (2006) Top-gathering periodic array derived from the self-organization of inorganic-organic hybrid pillars. *J Ceram Soc Jpn* 114:120–124.
40. Duan H, Yang JK, Berggren KK (2011) Controlled collapse of high-aspect-ratio nanostructures. *Small* 7(18):2661–2668.
41. Ovsianikov A, et al. (2008) Ultra-low shrinkage hybrid photosensitive material for two-photon polymerization microfabrication. *ACS Nano* 2(11):2257–2262.
42. Farsari M, Chichkov BN (2009) Materials processing: Two-photon fabrication. *Nat Photonics* 3(8):450–452.

Supporting Information

Hu et al. 10.1073/pnas.1503861112

S1. LPCS Setup and Process

An *xyz* piezoelectric nanotranslation stage (P545; Physik Instrumente) is used to trace out the pillar structures in the photoresist while the laser focus remains immobile. The objective, nanotranslation stage, and CCD camera for in situ observation are mounted in a modified optical microscope (BX51; Olympus). A mechanical shutter (SH05; Thorlabs) is used to control the beam during the material processing and the combination of a waveplate and a polarizer is used to attenuate the laser power. In the main text, an average power of 85 mW is applied for the pillar structures fabrication unless stated otherwise (measured before microscope, and it should be noted that the optics and objective in the microscope will cause a certain power loss). The detailed process is shown in Fig. S1. Photoresist is first drop-cast onto a cover glass and then baked on a hotplate at 100 °C for 1 h to remove solvents and form a gel. A femtosecond laser beam is used to irradiate the sample to fabricate the pillar array. After polymerization, the sample is developed in 1-propanol for 20 min. Then the sample is pulled out and the developer evaporates, during which the pillars assemble into ordered hierarchical structures with the aid of capillary force. Note that the total area of structures is determined merely by the translation stage; a long-range stage can be chosen to ensure the submicron pillars assemble into microscale cells over several centimeters and then large-area hierarchical structures can be generated by LPCS. Parallel laser printing techniques (1, 2) can also be used to ensure rapid fabrication across such a large area.

S2. Sample Characterization

The morphologies of the assembled microarchitectures are characterized by a field emission scanning electron microscope (Sirion 200; FEI). Before imaging, the samples are sputtered with a thin layer of gold. The fluorescent images of the structures are taken by an inverted microscope with fluorescence (DMI 3000B; Leica), where an excitation filter of 450–490 nm is used. The videos of the micropillar array self-organization and recovery are recorded by the Leica microscope in bright-field mode. The other optical characterizations of the samples and the in situ observations of microparticle trapping and releasing are performed on an Olympus BX51microscope.

S3. Quantitative Discussion on the Capillary Force, Elastic Restoring Force, Bond Number, and Effect of Gravity

In the main text we only discuss the forces in two critical cases (before the pillars bend and after their tips contact). Here we perform a quantitative study on the various forces during the pillar assembling process. The capillary force is given by $F_C = 2\pi\gamma r^2 \cos^2\theta/u$, where u is the distance between two pillar tips and dynamically changes when the pillars are bending. For the liquid 1-propanol, the interfacial tension $\gamma = 25.26$ mN/m. The radius of pillars $r = 380$ nm can be measured from SEM images. The distance between two pillar tips in the initial state is $u = d = 3$ μm. Thus, for a typical case of $\theta = 60°$, the capillary force is 1.91 nN when the pillars stand upright. The distance u decreases sharply as the pillars bend (it reaches zero when the top ends of two pillars contact) and hence the capillary force increases rapidly. According to previous studies (3, 4), it is reasonable to estimate the capillary force increases by more than three orders of magnitude at the last moment before two pillars contact (van der Waals interactions begin to take effect in nanometer scale). Thus, the maximum capillary force is probably ~2 μN. The elastic restoring force is given by $F_S = 3\pi E r^4 v/4h^3$, where v is the horizontal displacement of the pillar tip from its base. So, $F_s = 0$ when the pillar is upright at the beginning. For the photoresist SZ2080 used here, $E = 1\sim 2$ GPa (5). Therefore, the maximum elastic force F_s is 1.15~2.3 μN (when $v = d/2 = 1.5$ μm and $h = 4$ μm), which is comparable to the magnitude of the maximum capillary force. Hence, slightly tuning the geometry or the distribution of the pillars may induce controllable self-assemblies. Bond number is a dimensionless number to show the importance of surface tension forces compared with body forces (e.g., gravity) (6). Here $Bo = \rho g(d/2)^2/\gamma = 6.98 \times 10^{-7}$. The extremely small value ($\ll 1$) of the Bond number indicates that surface tension dominates the system and the effect of gravity is negligible. Specifically, the gravity of an individual pillar is around 1.8×10^{-5} nN, resulting in a torque $T_g \sim 1.4 \times 10^{-20}$ N·m on the pillars. The torque from the capillary force $T_c \sim 8 \times 10^{-12}$ N·m, is larger than T_g by eight orders of magnitude. Therefore, the effect of gravity can be neglected in this scale.

S4. Influence of the Microparticle on the Capillary Force Acting on Micropillars

When the particles are put into the solvent with pillar arrays, a number of particles drift into the designed cells and a new pillar–particle–pillar system is built, as shown in Fig. S5. A meniscus connecting the pillar and particle is formed, resulting in an extra capillary force. Because the distance between pillar and particle is very small, the pillar–particle capillary force is extremely strong. From the SEM images in Fig. 5B we can observe a slight difference between the shape of assembled cells with a particle and the empty ones, caused by the relatively strong pillar–particle capillary force. More obvious difference can be observed in Fig. S5. This phenomenon actually further benefits the trapping efficiency because the new capillary force inside the cell makes it much easier to trap the particle.

1. Hu Y, et al. (2013) High-efficiency fabrication of aspheric microlens arrays by holographic femtosecond laser-induced photopolymerization. *Appl Phys Lett* 103(14):141112.
2. Lin H, Jia B, Gu M (2011) Dynamic generation of Debye diffraction-limited multifocal arrays for direct laser printing nanofabrication. *Opt Lett* 36(3):406–408.
3. Chandra D, Yang S (2009) Capillary-force-induced clustering of micropillar arrays: Is it caused by isolated capillary bridges or by the lateral capillary meniscus interaction force? *Langmuir* 25(18):10430–10434.
4. Pokroy B, Kang SH, Mahadevan L, Aizenberg J (2009) Self-organization of a mesoscale bristle into ordered, hierarchical helical assemblies. *Science* 323(5911):237–240.
5. Skarmoutsou A, et al. (2013) Nanomechanical properties of hybrid coatings for bone tissue engineering. *J Mech Behav Biomed Mater* 25:48–62.
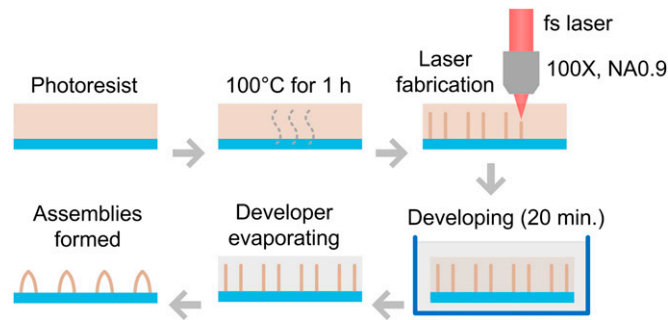6. Hager WH (2012) Wilfrid Noel Bond and the Bond number. *J Hydraul Res* 50(1):3–9.

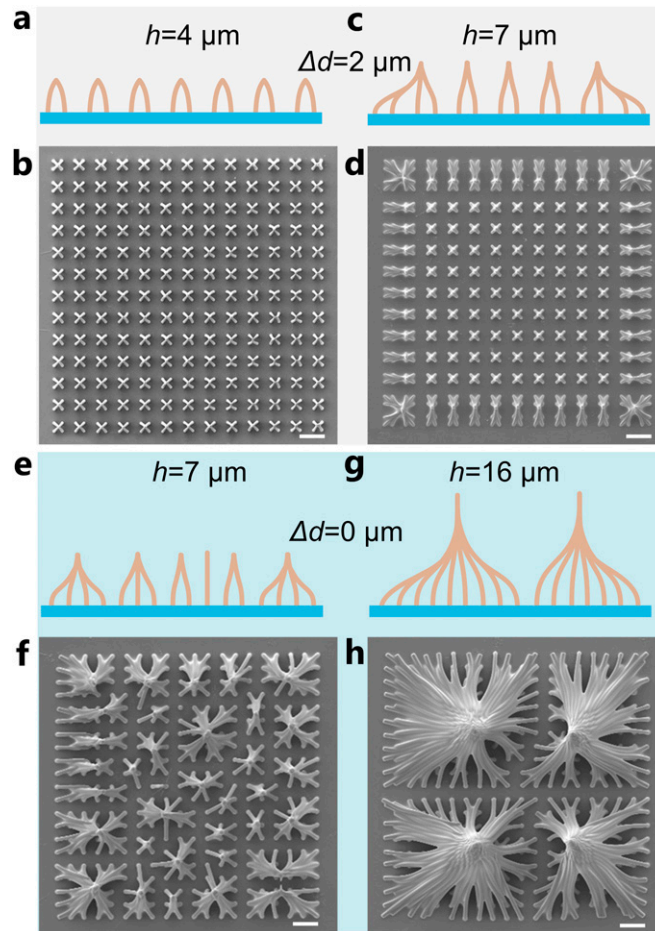**Fig. S1.** Scheme of the LPCS fabrication process.

Fig. S2. Schematic diagrams and SEM images of different assemblies when the conditions change. (*A* and *B*) $h = 4$ μm and $\Delta d = 2$ μm. A uniform four-pillar assembly is formed. (*C* and *D*) $h = 7$ μm and $\Delta d = 2$ μm. Boundary pillars assemble into 8- or 16-pillar cells owing to the larger capillary force. As the liquid dries, the evaporation front first reaches the boundary and forms a liquid drop around the array. The boundary pillars receive an asymmetric capillary force from the neighboring pillars and the substrates. The capillary force between the pillar and the substrate is much smaller than those between pillars and therefore the total force on boundary pillars is larger than central ones. (*E* and *F*) $h = 7$ μm and $\Delta d = 0$. Boundary pillars assemble into relatively larger unit cells than the central pillars and the assembly is random owing to the equal distance between pillars. (*G* and *H*) $h = 16$ μm and $\Delta d = 0$. Large filamentous aggregates with four nucleated centers are generated. (Scale bars, 10 μm.)
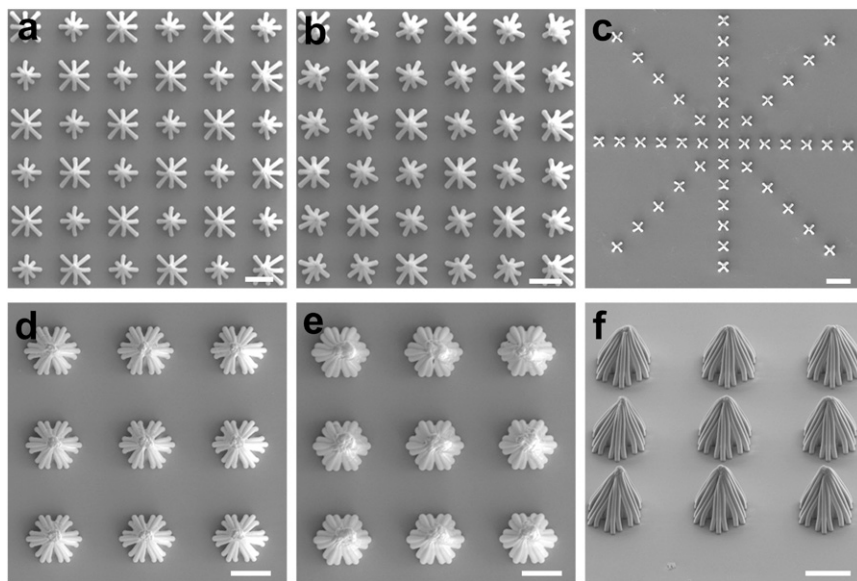
Fig. S3. Other examples of LPCS-prepared highly ordered self-assemblies. (*A*) Nine-pillar cells with different sizes and two rotation angles: 0° and 45°. (*B*) Nine-pillar cells with different sizes and three rotation angles: 0°, 30° and 60°. (Scale bars, 5 μm.) (*C*) Four-pillar cells are arranged in a pattern. (Scale bars, 10 μm.) (*D* and *E*) Daisy-like structures prepared using higher exposure power than those shown in Fig. 3: 95 and 115 mW, respectively. (*F*) Angled view of the daisy-like assemblies. (Scale bars, 10 μm.)
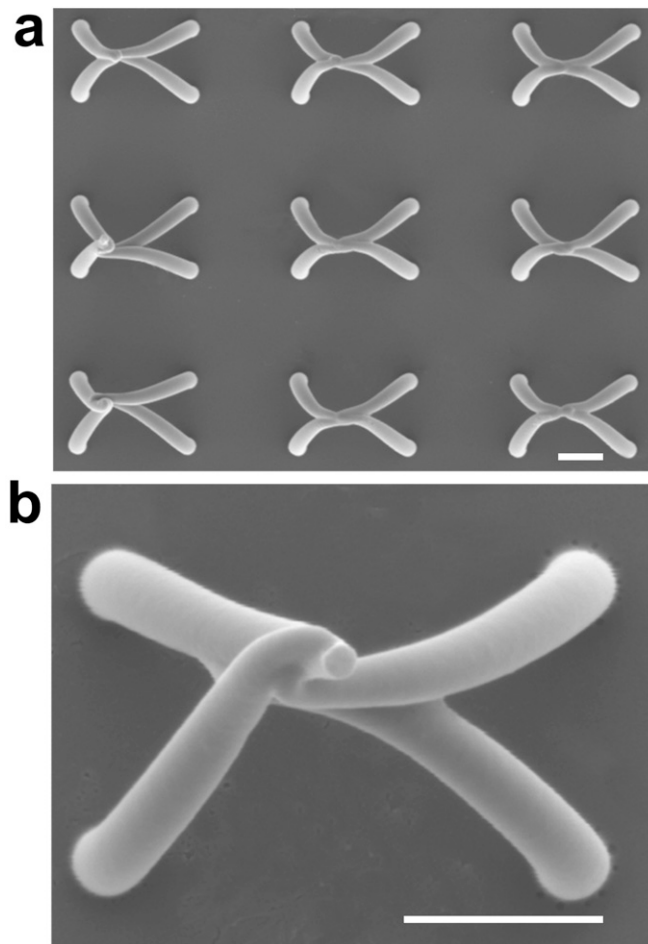

Fig. S4. SEM images showing the formation of helical patterns when increasing the pillar height. (*A*) The adjacent two-pillar cells further assemble into a four-pillar cell as the height of pillars is increased to 9 μm. (*B*) Magnified image showing the helical pattern beginning to appear. (Scale bars, 2 μm.)
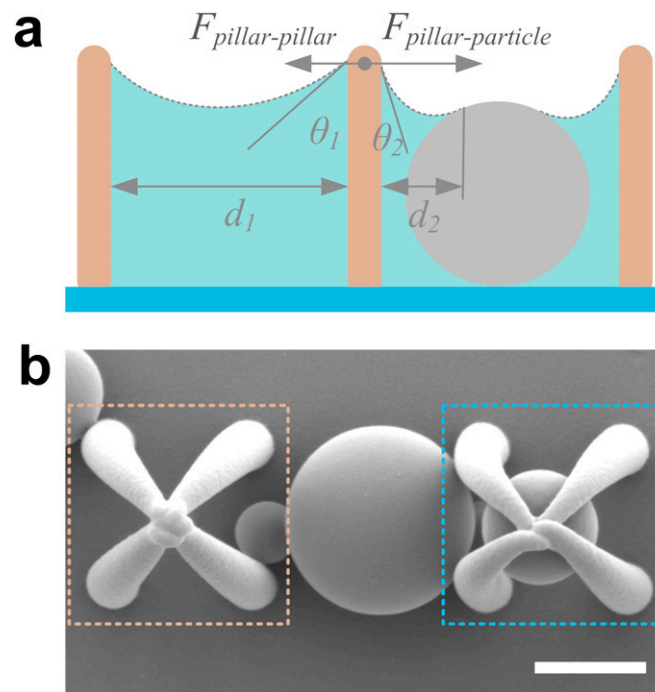
Fig. S5. (*A*) Schematic illustration of the geometry and forces in the pillar–particle–pillar system. The capillary force between pillars and particles $F_{pillar-particle}$ is larger than that between pillars and pillars $F_{pillar-pillar}$. (*B*) SEM image showing that the strong capillary force between pillars and particles may induce the configuration change of the assembled cells. (Scale bar, 2 μm.)
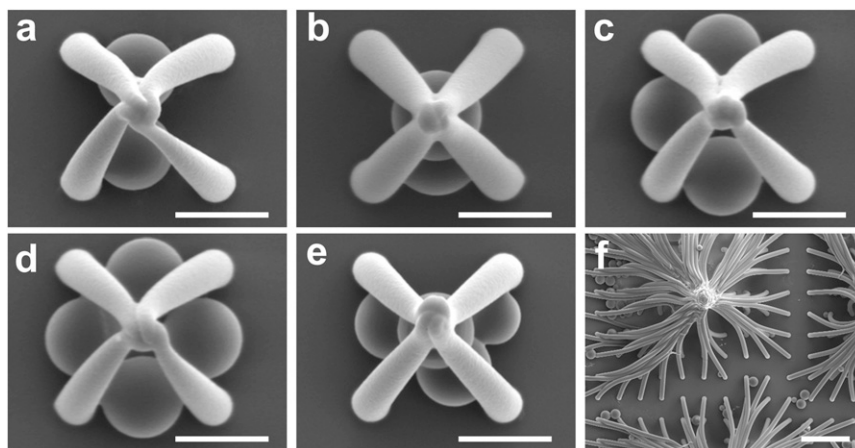

Fig. S6. (*A–E*) Large assembled cells may trap multiple particles at the same time. (Scale bars, 2 μm.) (*F*) Particles with different sizes can be trapped by the filamentous aggregates. (Scale bar, 10 μm.)
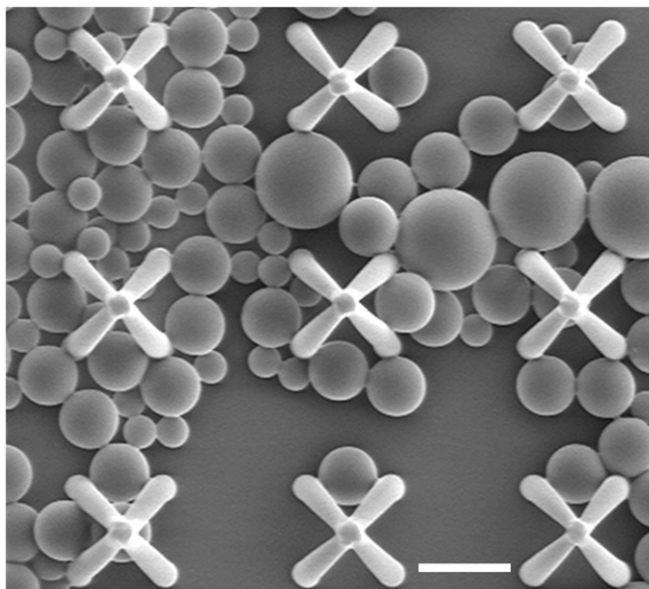
Fig. S7. High particle concentration results in aggregation. When the particle concentration is higher than 10^{-3} g/mL, the particles aggregate and trapping fails. Therefore, a concentration of 10^{-4} g/mL is used in the text. (Scale bar, 3 μm.)

Table S1. Summary of the yield percentage of assembled cells with different spacing variations and heights

Δd, μm height, μm	0.5, %	1.0, %	1.5, %	2.0, %	2.5, %	3.0, %
1	0	0	0	0	0	0
2	45	42	41	41	43	42
3	60	80.5	92	100	100	100
4	67	96	99	100	100	100
5	9.5	15.5	31	55	85	100
6	0	4.5	6.5	7	12.5	79
7	0	0	0	0	2.5	4

All of the data are obtained by optical microscope in situ observation.
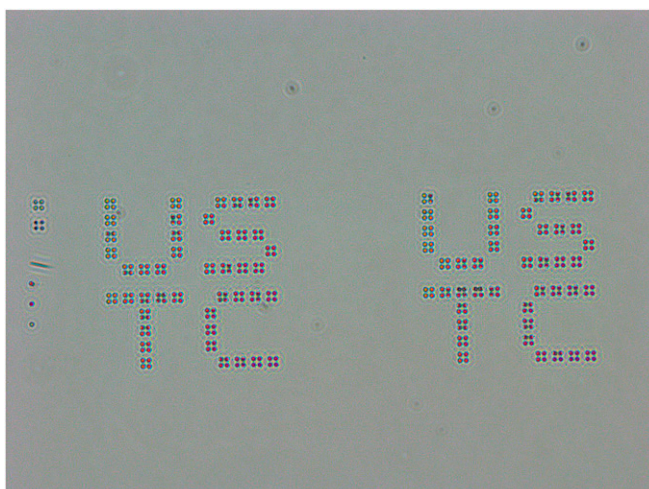
Movie S1. The reversible opening and closing of the assemblies. When the liquid evaporates, the pillars bend to form the assemblies. When the sample is immersed in liquid, the pillars return to their standing state and the assemblies open. The motion can be repeated for many cycles.

Movie S1